Effect of Phosphonate Monolayer Adsorbate on the Microwave Photoresponse of TiO₂ Nanotube Membranes Mounted on a Planar Double Ring Resonator

M. H. Zarifi,[1]* S. Farsinezhad,[1]* B. D. Wiltshire,[1] M. Abdorrazaghi,[1] N. Mahdi,[1] P. Kar,[1] M. Daneshmand[1] and K. Shankar[1, 2]

*Both authors contributed equally to the study

[1]Department of Electrical and Computer Engineering, University of Alberta, 9211 - 116 St, Edmonton, Alberta, Canada T6G 1H9

[2]NRC National Institute for Nanotechnology, 11421 Saskatchewan Dr NW, Edmonton, AB T6G 2M9

Authors to whom correspondence should be addressed:

1. Karthik Shankar (kshankar@ualberta.ca)

2. Mojgan Daneshmand (daneshmand@ualberta.ca)

Abstract

In this study, the effects of a phosphonate molecular monolayer adsorbed on the surface of a free-standing self-organized TiO_2 nanotube membrane, on the microwave photoresponse of the membrane are presented. This phenomenon is monitored using planar microwave sensors. A double ring resonator is utilized to monitor the permittivity and conductivity variation on the monolayer coated membrane and the sensor environment separately. It is shown that the rise time and subsequent decay of the amplitude (A), resonance frequency (f_0) and quality factor (Q) of the resonator depend on the existence and the type of the monolayer coating the membrane. Three different monolayers of n-decylphosphonic acid (DPA), 1H, 1H′, 2H, 2H′-perfluorodecyl phosphonic acid (PFDPA) and 16-phosphonohexadecanoic acid (PHA) adsorbed on the titania nanotube membrane are investigated while monitoring their microwave properties during the illumination time period and in the relaxation period, which demonstrate different behavior in comparison to each other and to the bare nanotube membrane layer. The effect of humidity on the TiO_2 nanotube membrane with and without different monolayers is also studied and the results demonstrate distinguishable microwave responses. While each of the monolayer-coated membranes exhibited an attenuation of the photo-induced change in A, f_0 and Q with respect to the bare membrane, PFDPA-coated membranes showed the smallest relative change in the monitored microwave parameters upon ultraviolet illumination and upon the introduction of different levels of humidity. These effects are explained on the basis of surface trap passivation by the monolayers as well as the hydrophobicity of the monolayers. Our work also shows how the interactions of self-assembled monolayers with charge carriers and surface states on metal oxides may be used to indirectly sense their presence through measurement of the microwave response.

1. Introduction

Self-assembled monolayers (SAM) can impact the surface properties of thin layers of semiconductors, metals and metal oxides in many ways including but not limited to, the insulation of conducting surfaces, performing biomolecular recognition, affording corrosion protection, imparting photosensitization, modification of electrode work functions, creating lyophobic and lyophilic surfaces, and as stabilizers and capping agents in the solution synthesis of thin films and nanomaterials [1-9]. The molecule constituting a self-assembled monolayer typically consists of an anchoring functional group (also called a head group), an aliphatic or aromatic backbone and a terminal functional group (also called end-group) at the end of the molecule opposite to the anchoring group. The anchoring group may be thiol, carboxylic acid, phosphonic acid, haloalkylsilanes, etc. and are respectively chemisorbed in an ordered manner on various surfaces such as gold, copper, nickel, silver, titanium dioxide, zinc oxide, silicon and silicon oxide [10]. Among the mentioned substrates, metal-oxides offer attractive possibilities for integration into microwave and millimeter devices [11]. Titanium dioxide (TiO_2) in comparison to other metal oxide materials is more favorable, due to its excellent resistance to corrosion by common acids, simple and fast functionalization process, and compatibility with many electrochemical and biological systems [12-15]. The TiO_2 surface can be functionalized using a variety of SAMs such as chlorosilanes, carboxylic acids, alkoxy- , phosphonic and phosphoric terminated acids which bond to the oxide surface through monodentate, bidentate or tridentate

chemisorption mediated by surface hydroxyl groups [13, 16, 17]. Carboxylate monolayers are reactive to hydrolysis while siloxane, hydroxamate, acetylacetonate and phosphonate monolayers are stable in aqueous conditions [18-22]. SAMs with a phosphonic acid functional group, not only create a strong binding to the surface but are also nontoxic, effective and stable which make them attractive for biosensing purposes [23]. However, the effect of SAM formation on the microwave properties of the resulting SAM-coated metal oxide film has received relatively little attention. Furthermore, a simple solution to verify the existence and quality of the SAM layers does not exist yet.

Due to the fact that the anatase phase of TiO_2 with the bandgap energy of 3.2 eV is an active ultraviolet (UV) radiation absorber, it is considered as a photoactive material. UV illumination promotes electrons from the valence band into the conduction band of TiO_2 while leaving positively charged holes behind. The competition between charge carrier generation, recombination and charge trapping in bulk and surface states together with the comparable dimensions of the nanotube wall-thickness and the minority carrier retrieval length make photoconductivity in TiO_2 nanotubes a complex phenomenon [24-30]. In a traditional semiconductor, the change in the conductivity due to bandgap illumination is given by [31]:

$$\Delta\sigma = e\left(\Delta n \mu_n + \Delta p \mu_p\right) \tag{1}$$

where σ is the conductivity, e is the electron charge, Δn and Δp are the densities of excess electrons and holes respectively, and μ_n and μ_p are the respective drift mobilities of electrons and holes. In addition to the photoconductive effect expressed by Eqn (1), the permittivity of the nanotubes is increased by UV illumination due to a trapping-related increase in bound charges (photodielectric effect). The photogenerated electron/hole pairs thus actively participate in the

conductivity and permittivity variation of the nanotube membrane. Meanwhile, their lifetime can be used as an indicator in microwave noncontact sensing purposes [32].

Microwave resonators have demonstrated promising operation for sensing applications in harsh and hazardous environments [33, 34]. Among different microwave sensor structures, planar sensors have demonstrated attractive performance for solid, liquid and gas material sensing [35-40]. In the reported applications, a single planar resonator has acted as the sensor core to detect or measure the variation of the electrical permittivity or conductivity of the analyte in the sensor vicinity. The dielectric properties of materials affect the electromagnetic field around the resonator and consequently change the electrical characteristics of the microwave resonator such as signal amplitude, resonance frequency and quality factor [41, 42]. In most reported sensors, during the sensing period, the ambient parameters such as temperature, pressure, humidity and other interference factors are either maintained constant or considered to be of negligible significance. The constant ambient assumption can be maintained in laboratory scale and controlled environment measurements. In real world applications, it is difficult to maintain the constant ambient condition which needs extra hardware and increases expenses. This will also increase the complexity of the system and limits the sensor application. To avoid the aforementioned complexities and increase the sensor reliability, a very powerful technique is to use the differential technique to measure the parameter variation.

Recently, we investigated the microwave response and photoresponse of bare TiO_2 nanotube array membranes, which indicated the strong influence of surface trap states and adsorbed oxygen [11, 32], which led to an examination of methods to mitigate both effects. The primary object of this work is therefore to understand the effect of adsorbed molecular monolayers on the microwave characteristics of TiO_2 nanotubes and a secondary objective is to develop an indirect

technique using double microwave resonators, UV illumination and photoconductivity for electrodeless, non-destructive low-cost monolayer detection on high surface area nanomaterials. Two planar microwave ring resonators are connected using two narrowband Wilkinson power dividers at their input and output ports. The nanotube membrane is placed on one resonator while the other one monitors the sensor's surrounding environment variation. Three different monolayers as well as different levels of the relative humidity are investigated. UV illumination is performed using a 254 nm curing lamp placed at a 20 cm distance above the nanotube membrane.

2. Microwave Planar Double Resonator Sensor Design

In order to have a differential measurement of the sensing parameters, a minimum of two sensors are required, wherein one measures the variation in the sensor environment (called the reference element) while the other measures the analyte and environment variation (called the sensing element). This technique enables sensitive measurements and distinguishes between the desired analyte monitoring and unknown environmental impact. To extract the absolute variation of an analyte material, extraction of the responses from the sensing element using the data from the reference element is required.

Fig. 1a shows the structure of a planar microwave sensor with a double resonator. Each resonator has a resonance frequency of 'f_1' and 'f_2' with a difference of 'Δf'. To guarantee a constant power delivery to each resonator, a power splitter/combiner is implemented at the input and output of the resonator array. An electromagnetic simulation of the designed structure is presented in Fig. 1c. The resonance frequency of each resonator depends on the length of the resonator ring as well as the ambient permittivity and conductivity near each resonator. To

achieve two resonance frequencies, Resonator1 (sensing resonator) has a longer length than Resonator2 (reference resonator) and consequently, has a lower resonance frequency than Resonator2. S-parameter simulation is also performed on the power divider to demonstrate the power transmission from port 1 to sub_port2 and sub_port3 which depicts an acceptable level of electromagnetic isolation between sub_port2 and sub_port3 to ensure the minimum loading effect from reference resonator to sensing resonator.
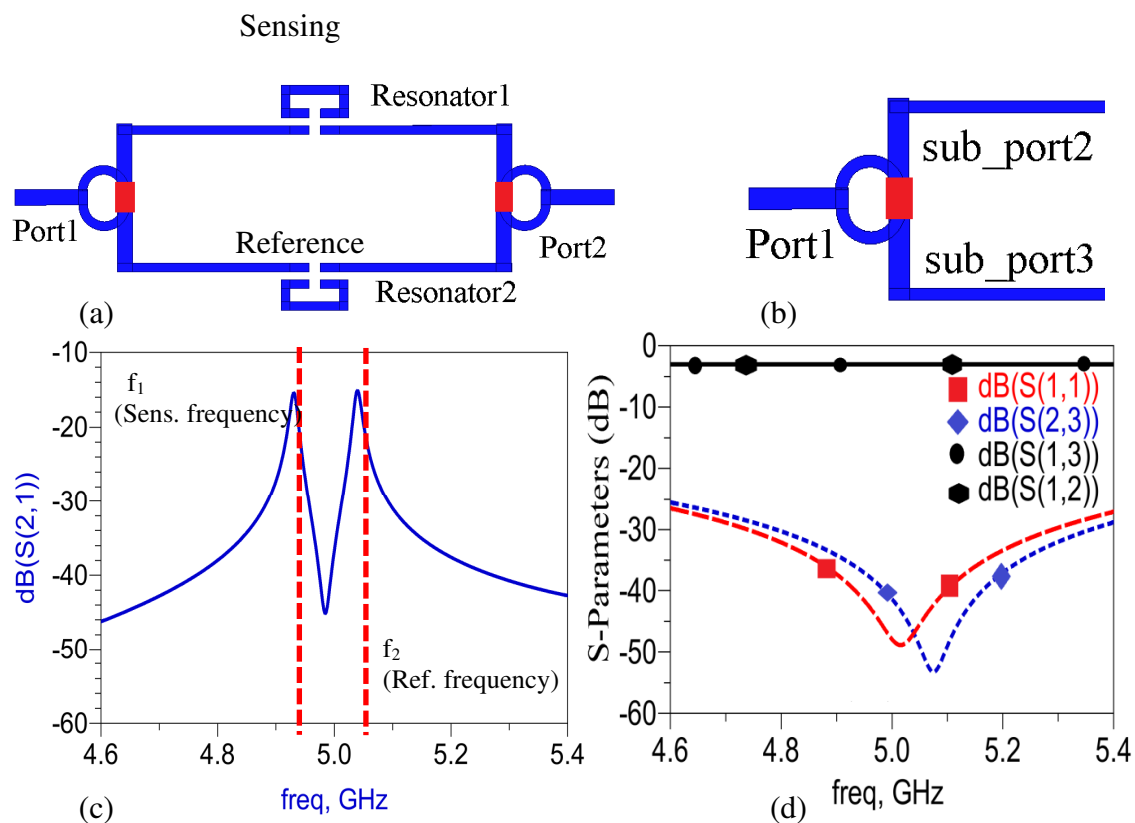
Fig. 1 Double resonator sensor structure for differential sensing application (a), Narrow-band power divider/combiner to divide the electromagnetic power equally between the resonators (b), double resonance resonant profile (c), power combiner analysis to demonstrate an acceptable level of isolation between the two resonators (d).

Two regions on planar microwave resonator sensors are more sensitive than other areas on the ring resonator. In these regions, because of the air gap and the discontinuity in the signal carrier microstrip lines, the electric field propagates out of the resonator substrate plane and this electric

field is utilized to perform the sensing around the resonator ambient. These most sensitive areas are demonstrated in Fig. 2a, as the capacitive gap between the input signal line and the resonator line (region 1) and a capacitive gap in the resonator loop (region 2). A sensitivity analysis is performed on these regions and the results of finite element method (FEM) analysis and circuit model simulation are presented in Fig. 2.

The electrical characteristics of the ambient (such as permittivity and conductivity) above the resonator plane in region 1, can be modeled by a parallel resistor and capacitor (R_c and C_c). The same RC model can be considered for the resonator gap in region 2 above the resonator plane (R_r and C_r). To compare the sensitivity of the sensor for C_c -C_r and R_c- R_r, the initial capacitor values were set to 0.005 pF and initial resistance values were set to 100 kΩ. The resonant profile was obtained and is presented in Fig. 2b. Then C_c was changed from 0.005 pF to 0.05 pF and R_c was changed from 100 kΩ to 10 kΩ while C_r and R_r were kept constant at 0.005 pF and 100 kΩ respectively. Furthermore, the same simulation was performed for C_r and R_r while C_c and R_c were kept at their initial values of 0.005 pF and 100 kΩ. It is clear that identical variation in C_r in comparison to C_c, and R_r to R_c, creates a larger frequency shift in resonance frequency with less degradation of the quality factor (Fig. 2b).

A sensitivity simulation was performed for capacitance (C_r and C_c) over a wide range of variation from 0.005 pF to 0.5 pF respectively and results are presented in Fig. 2c. It can be observed that the slope of the curve for region2 (C_r variation) is larger than the slope of the curve for sensitive region1 (C_c variation). Fig. 2c can also be a deceptive result since it shows the sensitivity of resonance frequency in region1 beyond 0.1 pF. This can be identified considering Fig. 2d, which shows that the quality factor drops tremendously below 50 for C_c > 0.1 pF due to which the sensor loses the resolution for those capacitance values.

According to the presented simulation results, the resonator sensor demonstrates more sensitivity to material in region 2 than region 1; therefore, this region is used as the TiO_2 membrane spot during the experiments.
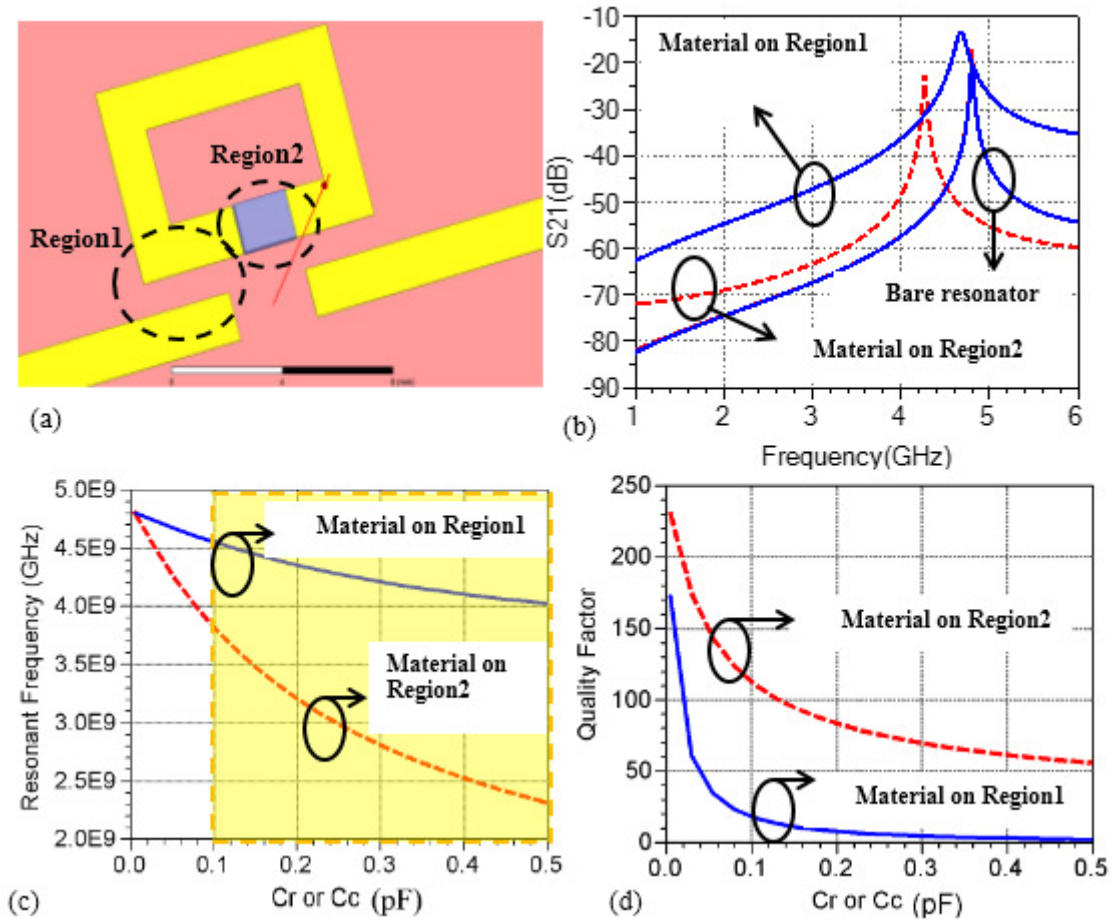
Fig. 2 (a) Two capacitive gaps in Region1 and Region2 on the ring resonator sensor (b) Resonant profile variation for capacitance variation in the sensitive regions (c) Comparison of the sensitivity of resonance frequency with respect to capacitance variation in Region1 and Region2 and (d) Study of the change in quality factor for capacitance change in Region1 and Region2.

3. Materials and Methods

3.1 Nanotube membrane preparation

A 0.89 mm thick titanium foil (99.9% purity) from Alfa Aesar was cut to form starting samples with particular working areas of 2 cm^2 and 0.25 cm^2. The samples were ultrasonically degreased in acetone (99.5%, from Fisher Scientific), methanol (99.8%, from Fisher Scientific), and DI water for 10 min each consecutively followed by drying with a nitrogen gun. The electrochemical anodization was performed in a two-electrode cell connected to a DC power supply with 2 cm^2 Ti foil as the working electrode and 0.25 cm^2 Ti foil as the counter electrode. The electrochemical anodization was conducted under a constant voltage (60 V) at room temperature in an ethylene glycol (99.9% from Fisher Scientific)-based electrolyte containing 4% H_2O and 0.3 wt% NH_4F (98.3% from Fisher Scientific). The distance between the working electrode and the counter electrode was 3 cm. The fabrication process of free-standing polycrystalline TiO_2 nanotube arrays (TNAs) began with electrochemical anodization for 72 hours followed by rinsing with methanol and water to remove the electrolyte and subsequent delamination of the TNAs from the substrate to form free-standing TNA membranes. Since the as-prepared free-standing TNAs were amorphous, thermal annealing was conducted at 360 ^{o}C in a programmable furnace for 14 hours with a 10 ^{o}C min^{-1} ramp rate in order to induce crystallinity. The annealing regimen was an optimized one designed to maximize the microwave photoresponse of the nanotubes. The as-prepared TNA membranes were functionalized by three different monolayers by self-assembly. n-decylphosphonate (DPA) and perfluorodecylphosphonate (PFDPA) monolayers were respectively formed by overnight immersion of the membranes in 1 mM solutions of DPA and PFDPA in methnaol. Monolayers of 16-phosphonohexadecanoic acid (PHA) were formed by overnight immersion of the

membranes in a 1 mM solution of PHA in a mixed solution of methanol and DI water (4:1 ratio). The DPA and PHA were purchased from Sigma Aldrich while the PFDPA was procured from Aculon Inc.

3.2 Measurement setup

The experiment consisting of UV illumination of the membranes and simultaneous microwave measurements was performed in a controlled chamber with a UV transparent quartz window, and temperature and humidity probes. The resonator sensor was placed inside the chamber and flexible microwave cables (RG-174) were used to connect the sensor to a vector network analyzer (Agilent E8362B PNA) . A constant temperature condition was established at 23 °C with tolerance of +/-0.5 °C. A bubbler container with a volume of 50 ml was filled with deionized water and kept at room temperature of 23 °C. The headspace above the water and inside the container was at 99.8 % RH. Dry air mixture with the headspace humidity was used to generate varying concentrations of humidity in the chamber both regulated using mass flow controllers. This setup provided the desired humidity, from 0.1% up to 95% RH. A Labview program was implemented for real-time data acquisition at controllable time intervals. The experimental setup schematic is shown in Fig. 3. A UV curing lamp with a wavelength of 254 nm was used to illuminate the nanotube membrane housed in the sensor chamber (intensity of 0.5 mWcm^{-2}).

3.3 Characterization

Electrochemical impedance spectroscopy (EIS) was performed at room temperature in a three-electrode electrochemical cell with a Ag/AgCl reference electrode and a platinum counter electrode, using a CHI 600D potentiostat (CH Instruments Inc.). The electrolyte was 0.15 M

KCl solution. Fourier transform infrared spectra (FTIR) were collected in diffuse reflectance mode (DRIFTS) using a ThermoNicolet Nexus FTIR Spectrometer.
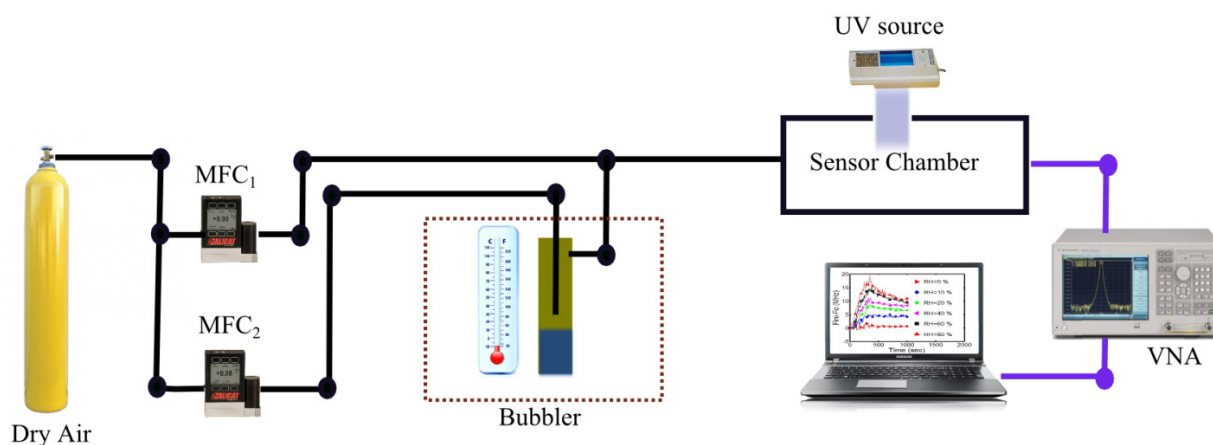
Fig. 3 Schematic illustration of the instrumentation and experimental setup for studying the effect of humidity on the microwave photoconductivity of TiO_2 nanotube membranes utilizing a passive microwave double resonator sensor.

4. Results and Discussions

To demonstrate the sensing performance of the double resonator sensor, a titania nanotube membrane was placed in the resonator gap in a temperature and humidity controlled environment. As demonstrated in the simulation results (Fig. 2c) this is the most sensitive region on the resonator sensor. The planar double resonator sensor is fabricated on a microwave substrate from Rogers Corporation (5880) with dielectric permittivity of 2.2 +/- 0.2, and a loss factor of 0.0009. The thickness of substrate and the copper conductive layers were 0.79 mm and 0.035 mm respectively. Fig. 4a shows the fabricated sensor in the controlled chamber with nanotube membrane mounted on the capacitive resonant gap. The 254 nm UV-lamp is placed out of the chamber in a distance of 20 cm from the sensor surface. UV-light penetrates through the quartz window and is incident on the TiO_2 nanotube membrane. The UV illumination is applied for 5 minutes and the data is automatically recorded every 10 seconds. UV light affects the

photoconductivity properties of the TiO_2 nanotube membrane by changing the permittivity and conductivity of the layer, the variation in which are represented through the alteration of the resonant profile. The main quantities describing the resonant profile are the resonant amplitude (A), resonance frequency (f_0) and quality factor (Q), which are also the parameters monitored by us. Fig. 4b shows the amplitude variation for the resonant profile comparing the sensor resonator amplitude and reference resonator amplitude during the UV illumination (shaded blue time period) as well as subsequent to illumination when the lamp is turned off. The reference resonator has no TiO_2 membrane layer on its resonant ring and therefore has less sensitivity to UV illumination while the resonator with the TiO_2 nanotube membrane in the coupling gap is very sensitive to UV illumination because of the change in the concentration of free and trapped charge carriers in the TiO_2 nanotubes during the test period.

Careful observation of the resonant profile and the resonance characteristics such as the maximum amplitude, resonance frequency and quality factor of reference resonator (blue lines in Fig. 4b-d), indicates a very small change during the UV-illumination, which can originate from lamp electrical noise, heat or change in the humidity in the immediate ambient of the reference resonator. One of the main advantages of using a double resonator is eliminating the environmental noise effect to purely track the UV influence on the TiO_2 nanotube membrane. At the same time, it is clear that the sensor resonator monitors the nanotube behaviour during both the exposure and relaxation time periods.
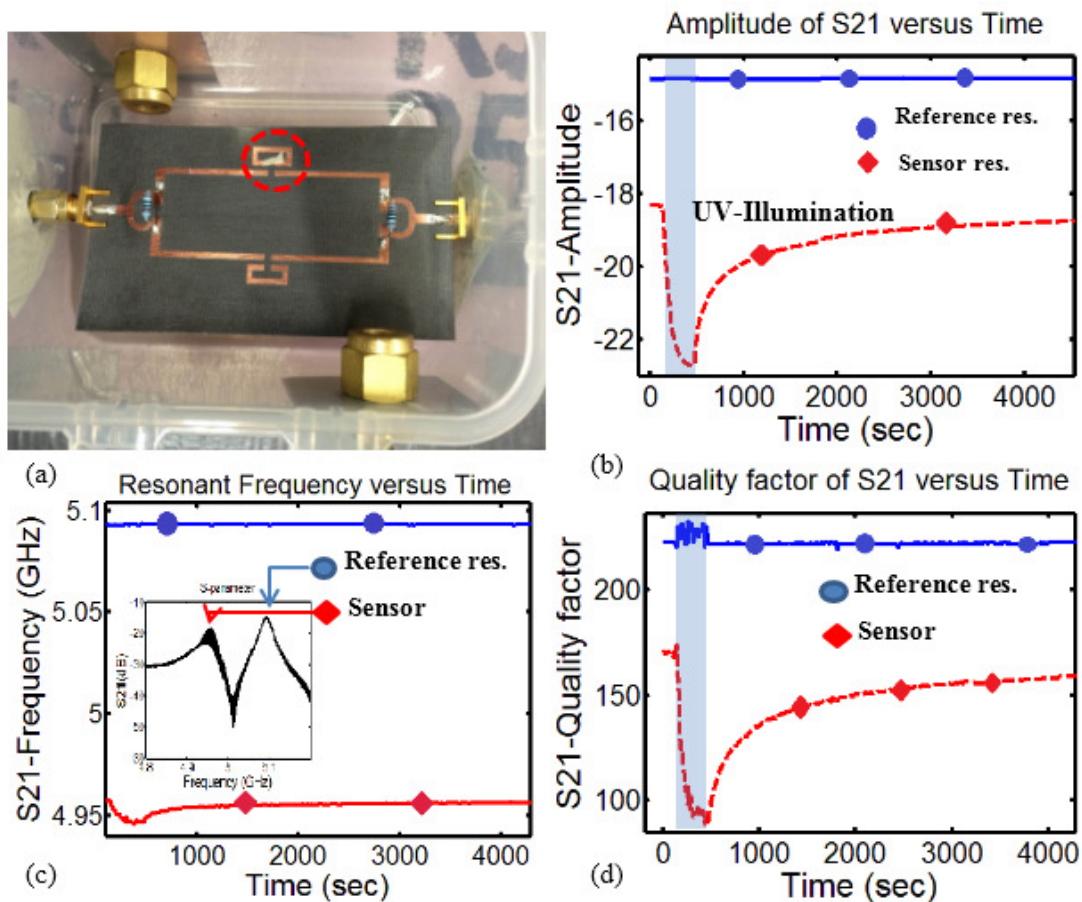
Fig. 4 (a) Implemented double resonator sensor with TiO₂ nanotube membrane (b) Resonant amplitude variation for two resonators with and without nanotube membrane prior to, during and following the UV illumination (c) resonance frequency variation during the time for both reference and sensor resonator in illumination process, double resonant profile is shown as inset and (d) Quality factor variation during the test period for reference and sensor resonator; an initial difference between all the resonance characteristics originated from the presence of the TiO₂ nanotube membrane sample in the coupling gap of the resonator.
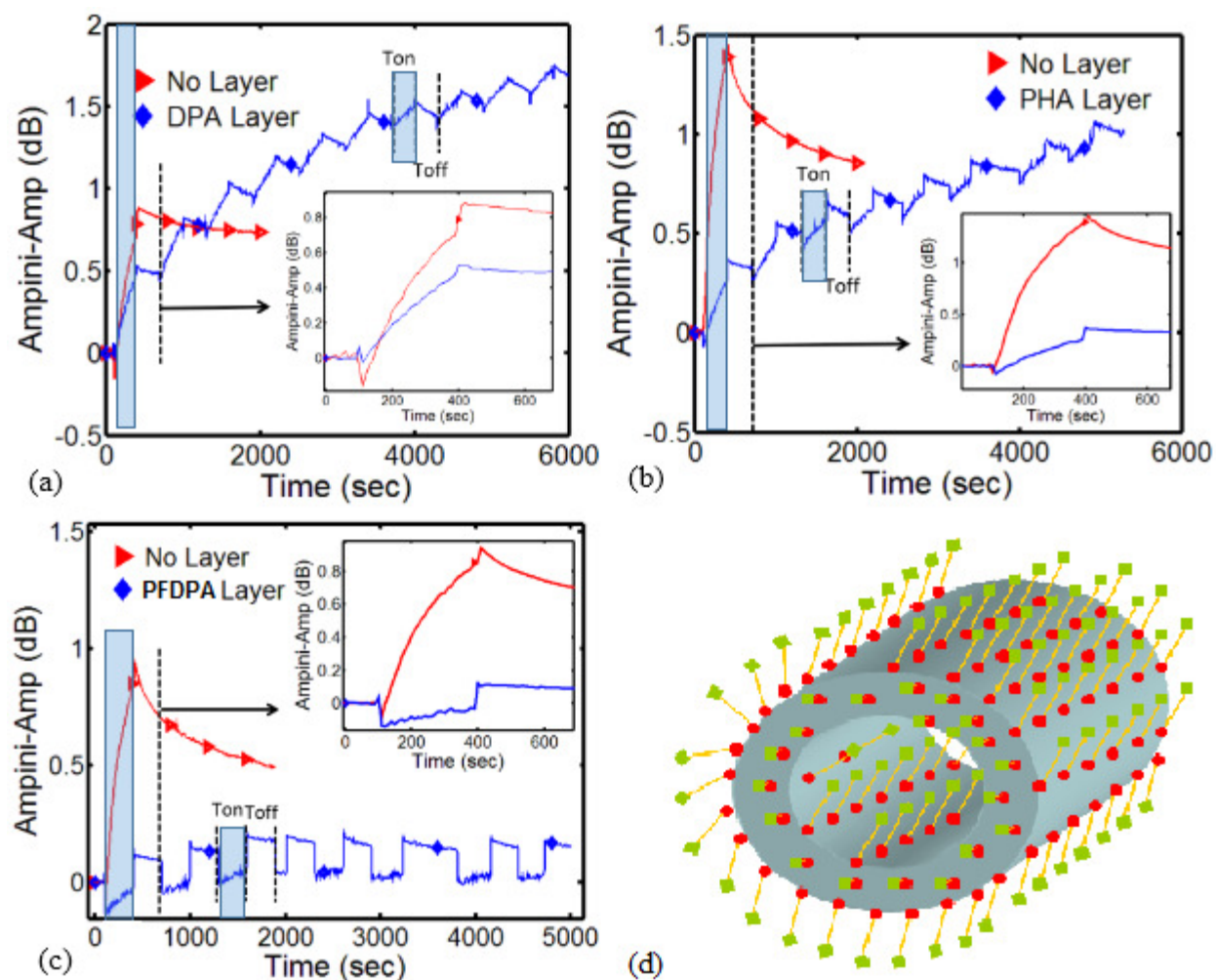
Fig. 5 Amplitude response of TiO₂ nanotube membranes coated with three different monolayers, Ampini is the resonant amplitude at time zero and Amp is the transient resonant amplitude (a) DPA (b) PHA and (c) PFDPA. For each monolayer, the transient response of resonant amplitude is presented before and after coating. $T_{on}=T_{off}=300$ seconds; (d) is a schematic illustration (not drawn to scale) of a single nanotube containing an adsorbed monolayer of a molecule with a headgroup shown in red and a tailgroup shown in green.
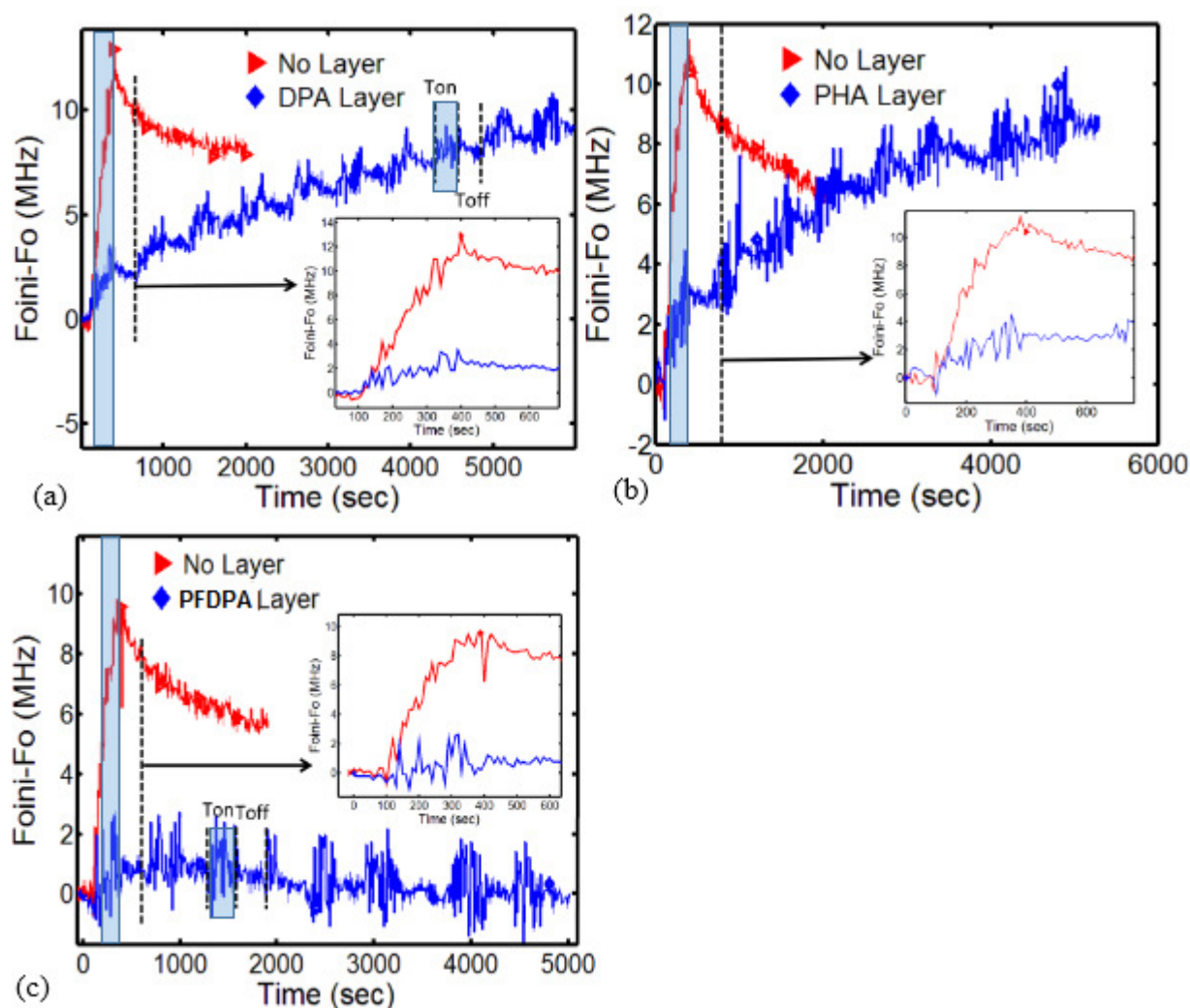
Fig. 6 Resonance frequency comparison between three different monolayers adsorbed on the TiO$_2$ nanotube membrane, Foini is the resonance frequency at time zero and Fo is the transient resonance frequency (a) DPA (b) PHA and (c) PFDPA. Each subfigure shows the membrane response before and after monolayer coating. T$_{on}$=T$_{off}$=300 sec.

The microwave response of free-standing TNAs membranes coated with three different monolayers of DPA, PHA and PDFPA was measured using the following protocol. Initially, a regular 5 minute UV illumination of the uncoated (bare) free-standing TNAs membranes is performed and the transient response of the specimens is recorded. Subsequently, the functionalization process is carried on the same samples and their transient response to a series of UV illumination pulses is recorded. Fig. 5 and Fig. 6 present the measured response for TNA

membranes coated with each of the three monolayers. Please note that we have previously verified the presence of the phosphonate monolayers on TiO_2 nanotube arrays using X-ray photoelectron spectroscopy (XPS) and Fourier transform infrared spectroscopy (FTIR), the details of which may be found elsewhere [7, 13]. It is clear from Fig. 5 that the overall amplitude change in TiO_2 nanotubes covered by a monolayer, is maximum for the DPA coating (closest to bare nanotube) and minimum for the PFDPA coating. A similar trend in frequency shift is also observed and shown in Fig. 6. For DPA-coated and PHA-coated TNA membranes, an accumulated frequency shift of up to 10 MHz is observed following eight illumination pulses whereas for PFDPA, the frequency shift is completely negligible. It is worth emphasizing the bare nanotube response to a single pulse (demonstrated in all the graphs for reference) and its complete distinction with the case with monolayer-coated TNA membranes. This behavior can be understood by considering electron trapping phenomena in TiO_2 nanotube arrays. It is well-known that in n-type metal oxide semiconductors such as TiO_2 and ZnO, atmospheric oxygen adsorbs on the semiconductor surface by trapping electrons to form oxide anions according to $O_2 + e^- \rightarrow O_2^-$ (*ads*) [25, 27, 28, 43]. Consequently, the concentration of free electrons in the nanotubes is decreased with concomitant band-bending due to the formation of a depletion region close to the nanotube surface. When the nanotube is illuminated by photons with energy exceeding the band gap of the semiconductor, free electrons and holes are created in pairs. A large fraction of the photogenerated holes are trapped at sub-ps timescales due to very fast hole traps in anatase TiO_2 [44]. A few more are lost to recombination with free and trapped electrons in the TiO_2 nanotube whose mobility-lifetime product has been measured to be ~10^{-4} $cm^2V^{-1}s^{-1}$ from steady-state DC photoconductivity measurements [25, 27, 28]. The remaining free holes are impelled towards the surface by the electric field in the depletion region. At the surface, the

holes desorb the oxide anions according to $O_2^-(ads) + h^+ \rightarrow O_2$ to liberate oxygen. Despite a substantial fraction of the photogenerated electrons also being captured by traps, the net concentration of free electrons increases in the nanotubes during the five minute-long illumination period as traps are filled and holes captured by the adsorbed oxide anions at the surface. These excess electrons absorb microwave radiation which manifests itself as a decrease in the amplitude of the microwave signal in comparison to the amplitude before light illumination accounting for the rise in the differential amplitude plots for bare (uncoated) TNA membranes in Fig. 6. Likewise, the resonance frequency shifts to lower values due to the increase in bound charges due to trapped charge carriers. However, for the monolayer coated TNA membranes, we observe a much smaller change in the amplitude and resonance frequency upon illumination. Even without UV illumination, the monolayers passivate the surface traps, displace the adsorbed oxide and release electrons trapped at the surface. Secondly, the photogenerated holes are not captured by the surface (because of fewer adsorbed oxide anions) and are now available for recombination with electrons in the nanotube. As a result, UV illumination produces a smaller change in conductivity for the SAM-coated membranes. The smaller change in frequency is due to the opposing effects of free electron plasma formation and carrier trapping on the permittivity [45]. The increasing frequency shift (i.e. a decreasing resonance frequency in comparison to the initial value) for DPA-coated and PHA-coated TNA membranes with successive illumination pulses with equal on and off cycle, indicates that the concentration of bound charges (trapped carriers) increases faster than their recombination and also faster than the increase in the free electron concentration (indicated by the amplitude increasing with successive illumination pulses in Fig. 5a and 5b) in these cases. On the other hand, the microwave response of PFDPA-coated TNA membranes changes very little even after

multiple illumination pulses which is highly suggestive of the dominance of carrier recombination processes over carrier trapping processes.
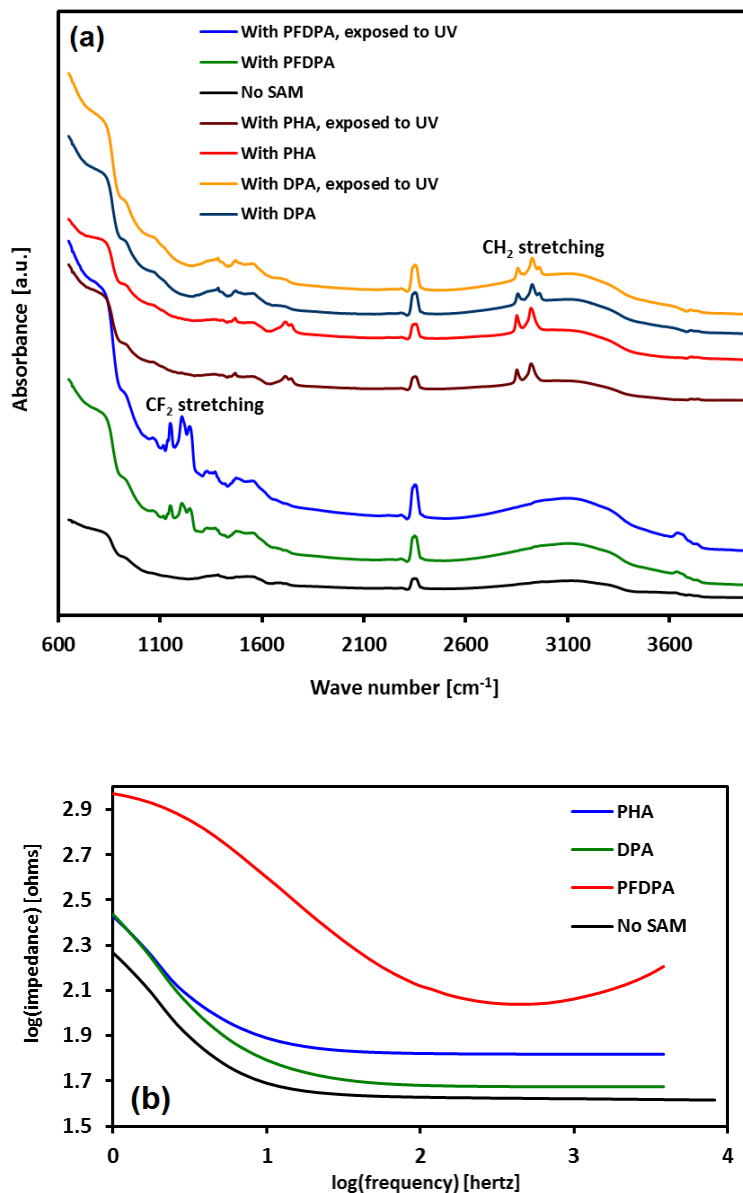
Fig. 7 (a) FTIR spectra for the TiO_2 nanotubes with PHA, PFDPA and DPA SAMs, and for bare nanotubes without SAM, before and after ten minute UV illumination and (b) EIS magnitude Bode plots for TiO_2 nanotubes coated with PHA, PFDPA and DPA SAMs, and for bare TiO_2 nanotubes without a monolayer coating.

We verified the stability of the three monolayers in response to UV illumination by performing Fourier Transform Infrared Spectroscopy (FTIR) before and after ultraviolet illumination by the same sources and for the same duration as used in the resonator sensor. FTIR spectra for the TiO_2 nanotubes with PHA, DPA and PFDPA SAMs and the same without SAM are shown in Fig. 7a. The peak at 2840 cm^{-1} is indicative of the symmetric stretching vibration mode of CH_2 while the peak at 2940 cm^{-1} is indicative of the asymmetric vibration mode of CH_2 [7]. The presence of the carboxylic acid group confirming the presence of 16-PHA is evident by the peak at 1694 cm^{-1} [7]. PFDPA is distinctly identified by the presence of bands at 1241, 1210 and 1152 cm^{-1}, which correspond to CF_2 stretching modes [13]. It is notable from Fig. 7a that the peak intensities of the SAM specific functional groups remain unaltered by UV exposure. Therefore on the basis of the FTIR spectra, it is reasonable to conclude that 10 minutes of UV exposure at an intensity of 0.5 mW cm^{-2}, from a 254 nm curing lamp, has no impact on the chemical composition or quality of the SAMs.

We performed Electrochemical Impedance Spectroscopy (EIS) on the TiO_2 nanotubes with and without the monolayers to quantify surface coverage. The principle of our estimation is that the presence of a self-assembled monolayer on the walls of the nanotubes reduces the total TiO_2 nanotube electrode area in contact with the liquid electrolyte thus reducing the interfacial capacitance. EIS Bode plots are shown in Fig. 7b for the TiO_2 nanotubes with PHA, DPA and PFDPA monolayers and the same without monolayers. As can be observed from **Fig 7b**, the impedance of the TiO_2 nanotubes with SAMs (PFDPA, DPA and PHA) exceed that for the blank TiO_2 nanotubes, thus constituting a clear distinction of the presence of SAMs.

$$\theta = 1 - \frac{z''_{\text{No SAM}}}{z''_{\text{With SAM}}} \tag{1}$$

The approximate surface coverage of the SAMs was quantified by using eq. (1) [46], where θ is the surface coverage of the SAM, in percentage, and is expressed in terms of the low frequency reactance of the blank nanotubes ($Z"_{No\ SAM}$), and the low frequency reactance of the nanotubes with SAMs ($Z"_{With\ SAM}$). The values of $Z"_{No\ SAM}$ and $Z"_{With\ SAM}$ were taken from the EIS data, and the calculated surface coverage values were found to be 48 %, 35 % and 32 % for the PFDPA, DPA and PHA SAMs respectively. Consistent with the surface coverage values, the low frequency capacitance values, as extracted from the EIS data, were 0.048 mF, 0.016 mF and 0.064 mF for PFDPA, DPA and PHA coated TiO_2 nanotubes respectively (samples of identical geometric area and nanotube dimensions were used), while the capacitance value for the TiO_2 nanotubes without SAM was 0.095 mF (i.e. greater than TiO_2 nanotubes with SAMs). The higher capacitance value for the nanotube sample without a SAM coating implied a higher surface area for the same compared to those with SAMs.

Humidity can interfere in photoconductivity measurements of metal oxide semiconductor nanostructures due its competing effect vis-a-vis oxygen on the trapping of charge carriers [47]. Therefore, we studied the effect of humidity variation in the controlled chamber by varying the relative humidity (RH) from 0 to 80% RH. The effect of RH on the microwave photoresponse of TiO_2 nanotube membranes is shown in Fig. 8. For every bare and monolayer coated membrane examined, the shift in f_0 increases as a function of RH, which indicates that the effect of RH on the number density of bound charges is stronger than the effect of illumination in increasing the free carrier density, which we attribute to the reported reactivity of water with both photogenerated electrons and holes [47]. Having an extra layer on the nanotube membrane can block the access of water molecules to the nanotube surface and consequently reduces the effect of RH on the UV illumination-induced dielectric property variation (permittivity and

conductivity) of the TNA membrane. The data in Fig. 8 demonstrates clearly that PFDPA-coated monolayers afford the strongest blocking action to water molecules as manifested by the negligibly small frequency shifts for different values of RH, which is attributed to their strong hydrophobicity. PHA on the other hand is moderately hydrophilic due to the presence of the terminal carboxylic acid endgroup, and while DPA is hydrophobic, some or all of the monolayer may be rendered hydrophilic by the ultraviolet illumination. This occurs because the terminal CH_3 groups in the DPA alkyl chain are vulnerable to oxidation to alcohols, aldehydes and carboxylic acids by the action of ultraviolet photons in the presence of air and moisture.
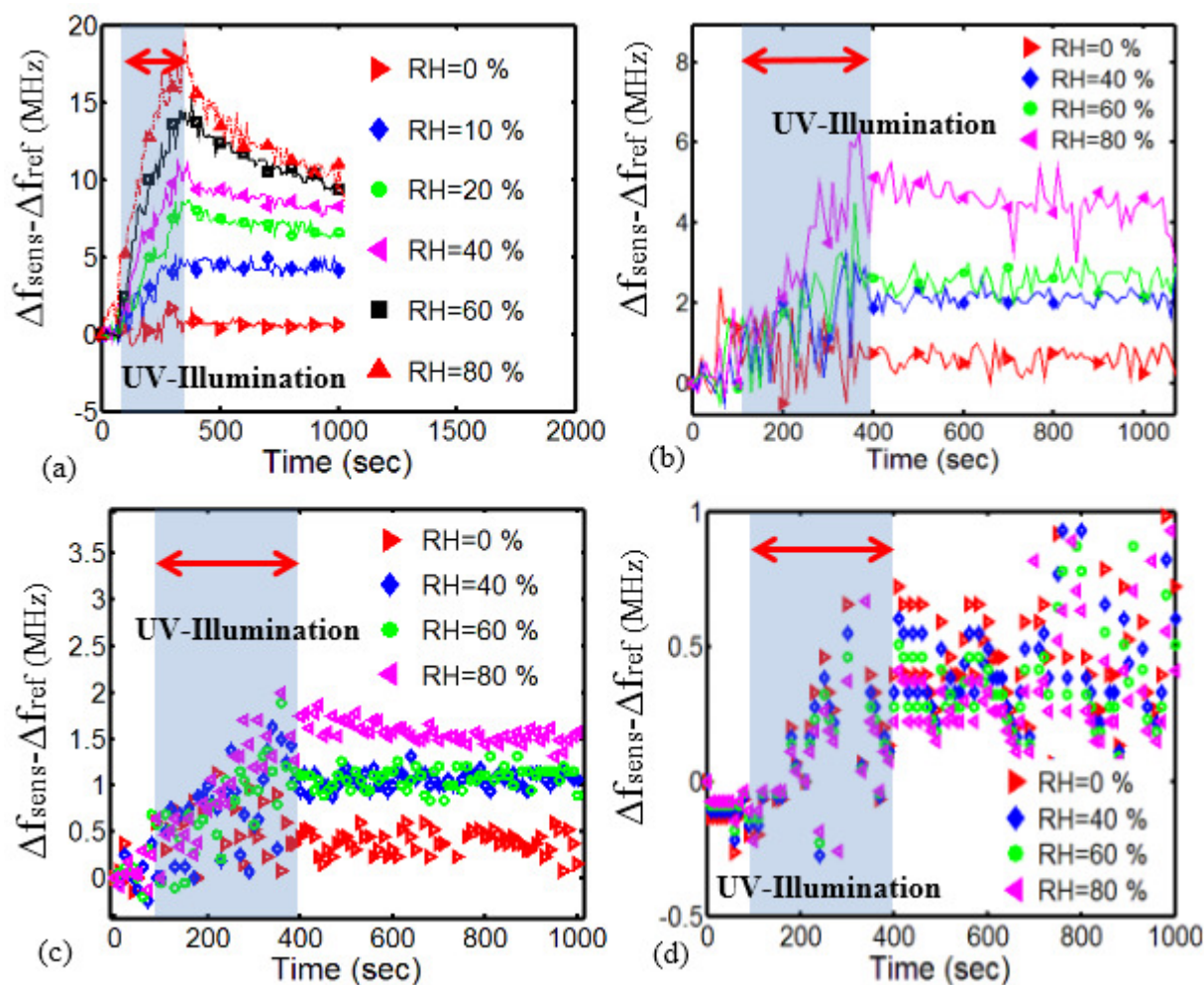
Fig. 8 Transient response of the sensor for different relative humidity in the controlled environment for (a) bare TNA membrane (b) PHA-coated TNA membrane (c) DPA-coated TNA membrane and (d) PFDPA-coated TNA membrane. An offset value of 136 MHz is extracted from the presented graphs for clearly demonstrating the results. This offset value originated from the presence of TiO_2 membrane on the sensing resonator and absence of that layer on the reference resonator.

The study here presents a basic concept and platform for direct monolayer sensing and detection. The results illustrate that benefiting from the distinct TiO_2 nanotube microwave photoconductivity response versus the assembled monolayer, one can develop selective monolayer sensors and analyzers. Secondly, our report is one of a new generation of papers [32, 48, 49] that views the high density of surface traps and other defects found in semiconductor nanostructures as a positive for sensing applications since it provides a opportunity to impart much needed selectivity in chemical and optical sensing. Both the nature of the passivating agent and the degree of passivation allow additional avenues to tailor the selectivity of the sensor response. Thirdly, although TiO_2 nanostructures coated with dye monolayers have been studied using time-resolved microwave conductivity in the context of charge transport measurements for dye-sensitized solar cells [50], the study of the microwave photoresponse of non-photoactive passivating SAM- coated metal oxide nanostructures has not been undertaken before and therefore fundamentally advances surface science.

5. Conclusion

Through a detailed study of the effect of three different self-assembled phosphonate monolayers on the microwave response of TiO_2 nanotube array membranes, a new indirect microwave photosensing method is reported for the detection of monolayers on high surface area nanoporous supports. The proposed technique is based on the combination of UV-illumination and the effect on the dielectric property variation of nanotube membranes resulting from the

photogeneration of electron-hole pairs, recombination, and trapping of the charge carriers. A planar double resonator sensor is considered as the transducer for detection of dielectric property changes on nanotube membrane. Having a planar passive structure reduces nonlinearity and temperature drift effect on the sensor while reducing the complexity of the sensor implementation. Additionally, having double resonators and using one as a reference and the other as the sensor resonator makes the sensor system more robust and reliable against the unwanted environmental noise. The proposed sensor structure operates in the microwave frequency span of 5 GHz. The impact of different relative humidity levels on the microwave photoresponse of bare and monolayer-coated TNA membranes are investigated and studied. All monolayers have a passivating action on surface traps. PFDPA-coated TNA membranes exhibit the smallest changes in signal amplitude and resonance frequency upon both UV illumination as well as UV illumination in the presence of varying humidity levels, which is attributed to the superior water molecule blocking action of the hydrophobic PFDPA monolayer. It has been also demonstrated that depending on the type of the monolayer, the microwave response of the membrane could change. It has been illustrated that the non-contact sensing method of the proposed sensor enables non-invasive measurements on fragile TiO_2 membranes tens of microns in thickness and also provides a way forward for the indirect detection of the presence of single monolayers of molecules anchored to high surface area nanomaterials.

Acknowledgements

References

[1] Adl A H, Kar P, Farsinezhad S, Sharma H and Shankar K 2015 Effect of sol stabilizer on the structure and electronic properties of solution-processed ZnO thin films *RSC Advances* **5** 87007-18

[2] Shuster M J, Vaish A, Szapacs M E, Anderson M E, Weiss P S and Andrews A M 2008 Biospecific Recognition of Tethered Small Molecules Diluted in Self‐Assembled Monolayers *Advanced Materials* **20** 164-7

[3] Grätzel M 2006 Photovoltaic performance and long-term stability of dye-sensitized meosocopic solar cells *Comptes Rendus Chimie* **9** 578-83

[4] de Boer B, Hadipour A, Mandoc M M, van Woudenbergh T and Blom P W M 2005 Tuning of Metal Work Functions with Self‐Assembled Monolayers *Advanced Materials* **17** 621-5

[5] Chinwangso P, Jamison A C and Lee T R 2011 Multidentate adsorbates for self-assembled monolayer films *Accounts of chemical research* **44** 511-9

[6] Farsinezhad S, Waghmare P, Wiltshire B D, Amiri S, Mitra S K and Shankar K 2014 The Wetting Behavior of TiO2 Nanotube Arrays With Perfluorinated Surface Functionalization*2014)*: American Society of Mechanical Engineers) p V009T12A71-VT12A71

[7] Kar P, Pandey A, Greer J J and Shankar K 2012 Ultrahigh sensitivity assays for human cardiac troponin I using TiO 2 nanotube arrays *Lab on a Chip* **12** 821-8

[8] Love J C, Estroff L A, Kriebel J K, Nuzzo R G and Whitesides G M 2005 Self-assembled monolayers of thiolates on metals as a form of nanotechnology *Chemical reviews* **105** 1103-70

[9] Ulman A 1996 Formation and structure of self-assembled monolayers *Chemical reviews* **96** 1533-54

[10] Jadhav S 2011 Self-assembled monolayers (SAMs) of carboxylic acids: an overview *Open Chemistry* **9** 369-78

[11] Zarifi M H, Mohammadpour A, Farsinezhad S, Wiltshire B D, Nosrati M, Askar A M, Daneshmand M and Shankar K 2015 Time-Resolved Microwave Photoconductivity (TRMC) Using Planar Microwave Resonators: Application to the Study of Long-Lived Charge Pairs in Photoexcited Titania Nanotube Arrays *The Journal of Physical Chemistry C* **119** 150615093503007-

[12] Pomorska A, Grundmeier G and Ozcan O 2014 Effect of Zn 2+ Concentration on the Adsorption of Organophosphonic Acids on Nanocrystalline ZnO Surfaces *Colloids and Interface Science Communications* **2** 11-4

[13] Farsinezhad S, Waghmare P R, Wiltshire B D, Sharma H, Amiri S, Mitra S K and Shankar K 2014 Amphiphobic surfaces from functionalized TiO 2 nanotube arrays *Rsc Advances* **4** 33587-98

[14] Wong E M, Hoertz P G, Liang C J, Shi B-M, Meyer G J and Searson P C 2001 Influence of organic capping ligands on the growth kinetics of ZnO nanoparticles *Langmuir* **17** 8362-7

[15] Ulman A 1991 Applications of LB and SA Films. Elsevier) pp 339-413

[16] Metoki N, Liu L, Beilis E, Eliaz N and Mandler D 2014 Preparation and Characterization of Alkylphosphonic Acid Self-Assembled Monolayers on Titanium Alloy by Chemisorption and Electrochemical Deposition *Langmuir* **30** 6791-9

[17]   Paz Y 2011 Self-assembled monolayers and titanium dioxide: From surface patterning to potential applications *Beilstein journal of nanotechnology* **2** 845-61

[18]   Iguchi N, Cady C, Snoeberger Iii R C, Hunter B M, Sproviero E M, Schmuttenmaer C A, Crabtree R H, Brudvig G W and Batista V S 2008 Characterization of siloxane adsorbates covalently attached to TiO2(vol 7034) p 70340C-C-8

[19]   McNamara W R, Snoeberger R C, Li G, Schleicher J M, Cady C W, Poyatos M, Schmuttenmaer C A, Crabtree R H, Brudvig G W and Batista V S 2008 Acetylacetonate Anchors for Robust Functionalization of TiO2 Nanoparticles with Mn(II)−Terpyridine Complexes *Journal of the American Chemical Society* **130** 14329-38

[20]   Brennan B J, Keirstead A E, Liddell P A, Vail S A, Moore T A, Moore A L and Gust D 2009 1-(3'-amino)propylsilatrane derivatives as covalent surface linkers to nanoparticulate metal oxide films for use in photoelectrochemical cells *Nanotechnology* **20** 505203

[21]   McNamara W R, Snoeberger Iii R C, Li G, Richter C, Allen L J, Milot R L, Schmuttenmaer C A, Crabtree R H, Brudvig G W and Batista V S 2009 Hydroxamate anchors for water-stable attachment to TiO2 nanoparticles *Energy & Environmental Science* **2** 1173-5

[22]   Brennan B J, Llansola Portoles M J, Liddell P A, Moore T A, Moore A L and Gust D 2013 Comparison of silatrane, phosphonic acid, and carboxylic acid functional groups for attachment of porphyrin sensitizers to TiO2 in photoelectrochemical cells *Physical Chemistry Chemical Physics* **15** 16605-14

[23]   Bae E and Choi W 2006 Effect of the anchoring group (carboxylate vs phosphonate) in Ru-complex-sensitized TiO2 on hydrogen production under visible light *The Journal of Physical Chemistry B* **110** 14792-9

[24]   Mor G K, Shankar K, Paulose M, Varghese O K and Grimes C A 2005 Enhanced photocleavage of water using titania nanotube arrays *Nano letters* **5** 191-5

[25]   Fàbrega C, Hernández-Ramírez F, Prades J D, Jiménez-Díaz R, Andreu T and Morante J R 2010 On the photoconduction properties of low resistivity TiO2 nanotubes *Nanotechnology* **21** 445703-

[26]   Richter C and Schmuttenmaer C A 2010 Exciton-like trap states limit electron mobility in TiO2 nanotubes *Nature Nanotechnology* **5** 769-72

[27]   Zou J, Zhang Q, Huang K and Marzari N 2010 Ultraviolet photodetectors based on anodic TiO2 nanotube arrays *The Journal of Physical Chemistry C* **114** 10725-9

[28]   Liu G, Hoivik N, Wang X, Lu S, Wang K and Jakobsen H 2013 Photoconductive, free-standing crystallized TiO 2 nanotube membranes *Electrochimica Acta* **93** 80-6

[29]   Mohammadpour A, Farsinezhad S, Wiltshire B D and Shankar K 2014 Majority carrier transport in single crystal rutile nanowire arrays *physica status solidi (RRL)-Rapid Research Letters* **8** 512-6

[30]   Mohammadpour A, Kar P, D Wiltshire B, M Askar A and Shankar K 2015 Electron Transport, Trapping and Recombination in Anodic TiO2 Nanotube Arrays *Current Nanoscience* **11** 593-614

[31]   Runyan W and Shaffner T 1998 *Semiconductor Measurements and Instrumentation*: New York, McGraw Hill)

[32]   Zarifi M H, Farsinezhad S, Abdolrazzaghi M, Daneshmand M and Shankar K 2016 Selective microwave sensors exploiting the interaction of analytes with trap states in TiO2 nanotube arrays *Nanoscale* **8** 7466-73

[33]   Nohlert J, Rylander T and McKelvey T 2015 Microwave resonator sensor for detection of dielectric objects in metal pipes: IEEE) p 914-9

[34]   Mason a, Korostynska O, Wylie S and Al-Shamma'a a I 2014 Non-destructive evaluation of an activated carbon using microwaves to determine residual life *Carbon* **67** 1-9

[35]   Abduljabar A A, Porch A and Barrow D A 2014 Real-time measurements of size, speed, and dielectric property of liquid segments using a microwave microfluidic sensor*2014/06//)*: IEEE) p 1-4

[36]   Naqui J, Durán-Sindreu M and Martín F 2011 Novel sensors based on the symmetry properties of split ring resonators (SRRs) *Sensors (Basel, Switzerland)* **11** 7545-53

[37]   Lee H-J, Lee J-H, Moon H-S, Jang I-S, Choi J-S, Yook J-G and Jung H-I 2012 A planar split-ring resonator-based microwave biosensor for label-free detection of biomolecules *Sensors and Actuators B: Chemical* **169** 26-31

[38]   Horestani A K, Naqui J, Shaterian Z, Abbott D, Fumeaux C and Martín F 2014 Two-dimensional alignment and displacement sensor based on movable broadside-coupled split ring resonators *Sensors and Actuators A: Physical* **210** 18-24

[39]   Sohrabi A, Shaibani P M, Zarifi M H, Daneshmand M and Thundat T 2014 A novel technique for rapid vapor detection using swelling polymer covered microstrip ring resonator. pp 1-4

[40]   Zarifi M H, Rahimi M, Daneshmand M and Thundat T 2016 Microwave ring resonator-based non-contact interface sensor for oil sands applications *Sensors and Actuators B: Chemical* **224** 632-9

[41]   Durán-Sindreu M, Naqui J, Paredes F, Bonache J and Martín F 2012 Electrically Small Resonators for Planar Metamaterial, Microwave Circuit and Antenna Design: A Comparative Analysis *Applied Sciences* **2** 375-95

[42]   Ebrahimi A, Withayachumnankul W, Al-Sarawi S and Abbott D 2014 High-Sensitivity Metamaterial-Inspired Sensor for Microfluidic Dielectric Characterization *IEEE Sensors Journal* **14** 1345-51

[43]   Lai C, Wang X, Zhao Y, Fong H and Zhu Z 2013 Effects of humidity on the ultraviolet nanosensors of aligned electrospun ZnO nanofibers *RSC Advances* **3** 6640-5

[44]   Tamaki Y, Furube A, Katoh R, Murai M, Hara K, Arakawa H and Tachiya M 2006 Trapping dynamics of electrons and holes in a nanocrystalline TiO 2 film revealed by femtosecond visible/near-infrared transient absorption spectroscopy *Comptes Rendus Chimie* **9** 268-74

[45]   Grabtchak S and Cocivera M 1998 Microwave response due to light-induced changes in the complex dielectric constant of semiconductors *Physical Review B* **58** 4701-

[46]   Bandyopadhyay K, Vijayamohanan K, Shekhawat G S and Gupta R P 1998 Impedance analysis of self-assembled naphthalene disulfide monolayer on gold using external redox probes *Journal of Electroanalytical Chemistry* **447** 11-6

[47]   Li Y, Della Valle F, Simonnet M, Yamada I and Delaunay J-J 2009 Competitive surface effects of oxygen and water on UV photoresponse of ZnO nanowires *Applied Physics Letters* **94** 23110-

[48]   Yu J, Wen H, Shafiei M, Field M R, Liu Z F, Wlodarski W, Motta N, Li Y X, Kalantar-zadeh K and Lai P T 2013 A hydrogen/methane sensor based on niobium tungsten oxide nanorods synthesised by hydrothermal method *Sensors and Actuators B: Chemical* **184** 118-29

[49]   Sarkar D, Ishchuk S, Taffa D H, Kaynan N, Berke B A, Bendikov T and Yerushalmi R 2016 Oxygen-Deficient Titania with Adjustable Band Positions and Defects; Molecular Layer Deposition of Hybrid Organic–Inorganic Thin Films as Precursors for Enhanced Photocatalysis *The Journal of Physical Chemistry C* **120** 3853-62

[50]   Katoh R, Huijser A, Hara K, Savenije T J and Siebbeles L D 2007 Effect of the particle size on the electron injection efficiency in dye-sensitized nanocrystalline TiO2 films studied by time-resolved microwave conductivity (TRMC) measurements *The Journal of Physical Chemistry C* **111** 10741-6